Indian monsoon and the elevated-heat-pump mechanism in a coupled aerosol-climate model

AGU PUBLICATIONS

JGR

Journal of Geophysical Research: Atmospheres

RESEARCH ARTICLE
10.1002/2015JD023346

Key Points:
- Use of a fully coupled aerosol-climate model for the aerosol-monsoon feedback
- Agreement with observation confirming the EHP and SDM effect on monsoon dynamics
- Potential impact on seasonal predictability of Asian monsoon

Correspondence to:
M. D'Errico,
miriam.derrico@cmcc.it;
miriam.derrico@yahoo.fr

Citation:
D'Errico, M., C. Cagnazzo, P. G. Fogli, W. K. M. Lau, J. von Hardenberg, F. Fierli, and A. Cherchi (2015), Indian monsoon and the elevated-heat-pump mechanism in a coupled aerosol-climate model, *J. Geophys. Res. Atmos.*, *120*, 8712–8723, doi:10.1002/2015JD023346.

Received 5 MAR 2015
Accepted 3 AUG 2015
Accepted article online 6 AUG 2015
Published online 5 SEP 2015

Indian monsoon and the elevated-heat-pump mechanism in a coupled aerosol-climate model

Miriam D'Errico[1,2], Chiara Cagnazzo[3], Pier Giuseppe Fogli[2], William K. M. Lau[4], Jost von Hardenberg[5], Federico Fierli[3], and Annalisa Cherchi[2,6]

[1]Ca' Foscari University, Venice, Italy, [2]Centro Euro-Mediterraneo sui Cambiamenti Climatici, Bologna, Italy, [3]Istituto di Scienze dell'Atmosfera e del Clima-CNR, Rome, Italy, [4]Earth System Science Interdisciplinary Center, University of Maryland, College Park, Maryland, USA, [5]Istituto di Scienze dell'Atmosfera e del Clima-CNR, Torino, Italy, [6]Istituto Nazionale di Geofisica e Vulcanologia, Bologna, Italy

Abstract A coupled aerosol-atmosphere-ocean-sea ice climate model is used to explore the interaction between aerosols and the Indian summer monsoon precipitation on seasonal-to-interannual time scales. Results show that when increased aerosol loading is found on the Himalayas slopes in the premonsoon period (April–May), intensification of early monsoon rainfall over India and increased low-level westerly flow follow, in agreement with the elevated-heat-pump mechanism. The increase in rainfall during the early monsoon season has a cooling effect on the land surface. In the same period, enhanced surface cooling may also be amplified through solar dimming by more cloudiness and aerosol loading, via increased dust transported by low-level westerly flow. The surface cooling causes subsequent reduction in monsoon rainfall in July–August over India. The time-lagged nature of the reasonably realistic response of the model to aerosol forcing suggests that absorbing aerosols, besides their potential key roles in impacting monsoon water cycle and climate, may influence the seasonal variability of the Indian summer monsoon.

1. Introduction

Aerosols significantly affect the Earth's radiation budget and climate at both global and regional scales. Aerosol influence occurs through scattering and absorbing radiation (direct effect) and through modifying microphysical cloud properties (indirect effect) [*Ramanathan et al.*, 2001]. Over South Asia, many recent studies have documented that aerosols in the atmosphere have a strong effect on regional climate and on monsoon precipitation [e.g., *Ramanathan et al.*, 2001]. Among the possible pathways coupling aerosol-monsoon interactions, *Lau et al.* [2006] and *Lau and Kim* [2006] have proposed that absorbing airborne particulate can directly impact monsoon rainfall through the elevated heat pump (EHP) mechanism. According to this hypothesis, shortwave heating, due to accumulated carbonaceous and dust aerosols over northern India and over the foothills of the Himalayan Plateau during the premonsoon season, may induce anomalous heating in the middle and upper troposphere. This heating, through atmospheric latent-heating feedback, results in a strengthened meridional tropospheric temperature gradient leading to increased monsoon rainfall. More recently, *Lau and Kim* [2010] have also suggested that increased rainfall at the monsoon early stage could cause reduced rainfall in the latter part of the monsoon season. In fact, they have interpreted the observed reduced rainfall trends over the Indian subcontinent in July and August, as a secondary effect of the EHP hypothesis. Indeed, an increase in rainfall and cloudiness in the early monsoon can cool down the surface, reducing the north-south temperature gradient and thus leading to a reduction in rainfall also in the late monsoon season. Moreover, an increase in low-level westerly flow associated to the EHP mechanism at the beginning of the monsoon season can also transport more dust from the western deserts, thus sustaining surface cooling via a reduction of solar radiation reaching the soil (the solar dimming effect (SDM) [*Ramanathan et al.*, 2005]).

Implications for the EHP hypothesis and the subsequent contribution to SDM are potentially very large, ranging from a better understanding of climate variability to a better estimate of climate predictability at the seasonal, interannual to longer time scales over South Asia [*Turner and Annamalai*, 2012]. *Lau and Kim* [2010] were in fact able to explain observed long-term trends in the Indian monsoon regional rainfall in terms of the EHP theories on the atmospheric diabatic heating associated with absorbing aerosols and its subsequent contribution to the solar dimming effect.

General circulation models of the atmosphere and coupled atmosphere-ocean models have been used to estimate the effect of the direct radiative forcing by aerosol on the Indian summer monsoon [e.g., *Meehl et al.*, 2008; *Collier and Zhang*, 2009; *Menon et al.*, 2002; *Wang et al.*, 2009]. Some recent modeling studies have found that anthropogenic and biomass burning aerosols may induce a reduction in observed precipitation over most parts of the Indian subcontinent in summer monsoon [e.g., *Bollasina et al.*, 2011; *Ganguly et al.*, 2012]. Although there is observational evidence of the EHP hypothesis at several time scales [*Lau et al.*, 2006, 2008] and confirmation of this theory by several modeling works [e.g., *Huang et al.*, 2007; *Meehl et al.*, 2008; *Randles and Ramaswamy*, 2008] there is still an open debate about a full understanding of the mechanism based on observations and model simulations [*Nigam and Bollasina*, 2010; *Lau and Kim*, 2011]. Part of the discrepancy among the interpretation of the EHP mechanism in different model simulations has been attributed to the absence of an interactive ocean [*Bollasina and Nigam*, 2008], of aerosol indirect effect, and of a realistic aerosol vertical distribution [*Kuhlmann and Quaas*, 2010].

It is therefore necessary to consider the feedback deriving from a full coupling of an atmosphere-aerosol general circulation model to a dynamical ocean and sea ice model. A few of the latest generation climate models used for climate predictions and projections, including an interactive coupling among atmosphere-ocean and sea ice components of the climate system, as, for example, the ones used for the Coupled Model Intercomparison Project Phase 5 (CMIP5) exercise, include interactive aerosol modules. However, the majority of these models have shown large differences in representation of aerosol processes related with rainfall, depending on the particular model and microphysics parameterization used, even for the same initial and forcing conditions. In particular, recent studies [*Lebo and Seinfeld*, 2011; *Tao et al.*, 2012; *Fan et al.*, 2013] have shown large differences in simulating the aerosol effects on deep convection. A state of the art of models including aerosol schemes representing the global variation of microphysical processes is given by *Mann et al.* [2014]. Likely, improvements of cloud parameterization and related validations are needed for a better understanding of the role of aerosol-convection interactions in the development of the summer monsoon [*Lee et al.*, 2014].

In this study we examine the influence of aerosols on the Indian monsoon precipitation and circulation using the Centro Euro-Mediterraneo sui Cambiamenti Climatici (CMCC) coupled aerosol-atmosphere-ocean and sea ice climate model, based on the global climate-aerosol model ECHAM5-HAM for the atmospheric part. The experiment performed and analyzed has fixed present-day conditions for greenhouse gases, solar irradiance, and ozone but interactive aerosols loading, including desert dust. The simulation also includes an interactive wind-driven desert dust emission scheme. The objective of this setup is to evaluate and understand the fundamental dynamical feedback between aerosols and the monsoon under conditions of constant anthropogenic forcing. Climate-aerosol interactions in India have been already studied with the global climate-aerosol model ECHAM5-HAM [*Henriksson et al.*, 2014]. That work considered a set of simulations with setups allowing the separate study of the effects of aerosol light absorption, total atmospheric effects of anthropogenic aerosols and possible effects of oceanic responses through mixed-layer ocean simulations and sensitivity analyses with modified fixed sea surface temperatures (SSTs). They conclude that aerosol light absorption increases rainfall in northern India but effects due to solar dimming and circulation work to cancel the increase. In our case we include an interactive ocean, in order to fully simulate the atmosphere-ocean feedback and we use composites considering strong minus weak aerosol loading years. As regional ocean aerosol-climate interaction is highly sensitive to models and/or model setup, this can be considered an important and independent study that supports EHP.

This paper is organized as follows: section 2 describes the model used and the design of the numerical experiment. Section 3 presents the main results of the analysis in terms of the impact of aerosols loading on the Indian summer monsoon precipitation and circulation, separating early and late monsoon season, to verify the EHP mechanism hypothesis. Finally, section 4 discusses the main conclusions of the study.

2. Model, Experimental Setup, and Reanalysis/Observations Used for Comparison

2.1. The Coupled Model

The model used in this study is an atmosphere-aerosol-ocean-sea ice coupled model consisting of ECHAM5 [*Roeckner et al.*, 2006] as atmospheric component, OPA 8.2 [*Madec et al.*, 1999] as oceanic component, LIM2 [*Timmermann et al.*, 2005] as sea ice model, and the HAM module for aerosols [*Stier et al.*, 2005], all

interactively coupled (namely, the CMCC aerosol climate model). The software used to couple the atmosphere (including the aerosols) and the ocean components is OASIS3 [*Valcke*, 2006]. Basically, the atmosphere-ocean-sea ice coupled components are the same of the state-of-the-art CMCC-CM coupled model [*Scoccimarro et al.*, 2011; *Fogli et al.*, 2009], but here the atmosphere is at lower resolution and interactively coupled with an aerosol module. In this study ECHAM5 is used with six shortwave radiation bands [*Cagnazzo et al.*, 2007] and a horizontal resolution at triangular truncation T63 with 31 vertical levels and the top of the atmosphere at 10 hPa. OPA8.2 is a primitive equation ocean general circulation model that is numerically solved on a global ocean curvilinear grid known as ORCA [*Madec and Imbard*, 1996]. Here we use ORCA2, with a resolution of 2° of longitude and a variable mesh of 0.5–2° of latitudes from the equator to the poles. The vertical grid has 31 levels (the 31st level is below the bottom) with variable layer depth and a constant 10 m step in the top 100 m. The aerosol module HAM has a prognostic representation of the composition, size distribution, and mixing state of the major global aerosol components: sulphate, black carbon (BC), particulate organic matter, sea salt, and mineral dust (DU) [*Stier et al.*, 2005, 2007]. The module predicts the evolution of an ensemble of microphysically interacting internally and externally mixed aerosol populations. Table 1 of *Stier et al.* [2005] shows the ranges of the modes together with the aerosol typologies. The microphysical core is M7 that considers the processes of coagulation, condensation on preexisting aerosols, aerosol nucleation, thermodynamical equilibrium with water vapor, and the intermodal transfer. The prognostic treatment of size-distribution, composition, and mixing state allows the explicit calculation of the aerosol optical properties with the Mie theory [*Toon and Ackerman*, 1981]. The calculation is precomputed for 24 solar spectral bands (otherwise too computationally expensive) and supplied in look-up tables with the three dimensions: Mie size parameter and real and imaginary part of the refractive index. The look-up table procedure provides extinction cross section, single scattering albedo, and asymmetry factor for each mode. Differently from *Stier et al.* [2005], the values from the 24 solar spectral bands are mapped to the six solar ECHAM5 bands and not the four bands. The parameters for the seven aerosol modes are then combined to provide the necessary input to the ECHAM5 radiation scheme. Analytical solutions are applied to integrate the aerosol dynamics equation for each mode, calculating the updated aerosol numbers and the transfer between the modes. From the analytically integrated changes in the aerosol numbers, the corresponding aerosol mass concentrations are calculated mass conserving by summing up the number of particles transferred between the modes and multiplication with the respective mean particle masses. More details are given in *Stier et al.* [2005]. The lifetime is estimated as the ratio of the column burden to the total source: the BC lifetime is 5.4 days and the lifetime for DU is 4.6 days as reported in *Stier et al.* [2005] (their Table 5). The scheme for dust emissions is based on *Tegen et al.* [2002, 2004], while that of sea-salt emissions is based on *Schulz et al.* [2004]. For black and organic matter, fossil fuel and biofuel [*Bond et al.*, 2004], vegetation fires [*Van Der Werf et al.*, 2003], and biogenic emissions are used. The aerosol properties generated from the ECHAM5-HAM coupling have been analyzed in detail in previous works: the model is able to simulate anthropogenic aerosol concentrations and aerosol optical depths reasonably well [*Folini and Wild*, 2011; *Henriksson et al.*, 2011; *Stier et al.*, 2005, 2007]. In this study the aerosol single scattering albedo, i.e., the ratio of the extinction due to scattering to the total extinction due to scattering and absorption, is derived from Aerosol Robotic Network [http://aeronet.gsfc.nasa.gov; *Holben et al.*, 1998; *Dubovik and King*, 2000; *Holben et al.*, 2001].

2.2. Experimental Setup

A long simulation representing the present climate has been conducted, with oceanic initial conditions derived from a stable control simulation (about a thousand of years). In this study, we analyze the last 80 years of this experiment with external forcings kept constant (fixed to conditions typical for the year 2000). Forcings include the concentrations of well-mixed green-house gases and incoming solar irradiance for year 2000 from the CMIP5 forcing data. The seasonally varying ozone distribution is repeated every year and is based on the 2000 year climatology. For aerosols, the emission data set is based on the Aerosol Comparisons between Observations and Models (AeroCom) aerosol model intercomparison project inventories for the year 2000 [*Dentener et al.*, 2006].

In our experiment the indirect effect of aerosols is not included. As in this study we basically want to verify the EHP hypothesis that refers to the role of absorbing aerosols (dust and black carbon) in intensifying the Indian monsoon precipitation [*Lau et al.*, 2006]; we will consider only those types of aerosols in our analysis. For a validation of how the aerosol absorption optical depth (ABS) is reproduced in the model we refer to the extensive evaluation of the realistic skill of the ECHAM5-HAM coupling in *Stier et al.* [2005].

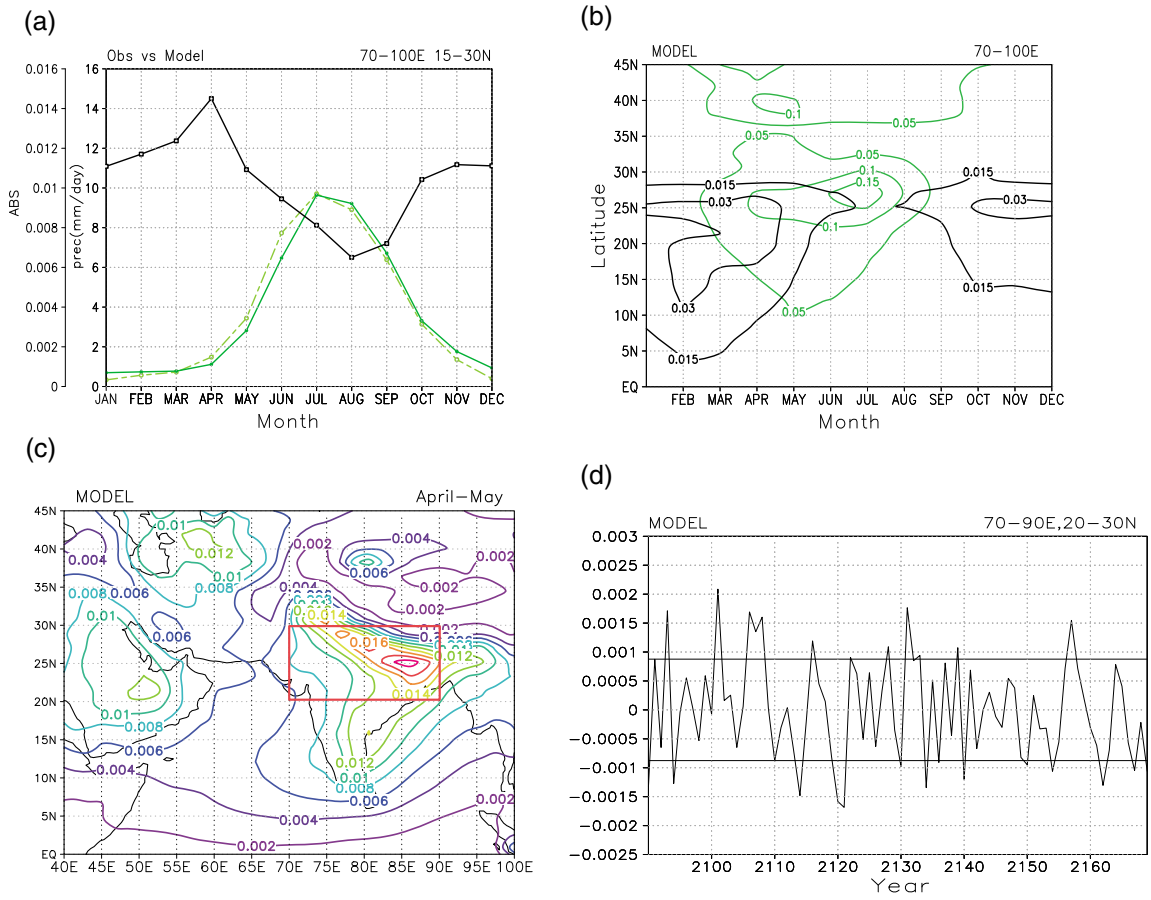

Figure 1. (a) Climatology of absorbing aerosols ABS (black line) and of total rainfall (mm d^{-1}) for the model (green solid line) and GPCP data set (green dashed line) over the region 70°E–100°E, 15°N–30°N. (b) Time-latitude evolution of aerosol optical thickness (ABS) of carbonaceous aerosols (black carbon and organic carbon, black line) and soil dust (green line), averaged over longitude from India to the Taklamakan desert (70°E–100°E). (c) Climatological distribution of aerosols absorption optical thickness over the Indian subcontinent and adjacent areas for April–May, with the red box indicating the region where the ABS index is defined. (d) Time series of standardized anomaly of ABS averaged over the area 20–30°N,70–90°E in April–May, for 80 years. The solid lines correspond to ±1 standard deviation.

2.3. Reanalysis and Observed Data Sets

The model climatology is compared with data from the ERA40 global atmospheric reanalysis product [*Uppala et al.*, 2005] and with the Global Precipitation Climatology Project (GPCP) gridded rainfall observational product, version2 [*Adler et al.*, 2003].

3. Results

We have proceeded to compare aerosol climatologies of our specific coupled simulation, with the aerosol climatologies derived from *Bucci et al.* [2013], showing data of aerosols (both dust and black plus organic carbon) frequency of occurrence in different seasons retrieved from Cloudsat satellite. Even if a direct quantitative comparison was not possible, by comparing their results with our model products we have found that the distribution of black and organic carbon together with dust is quite well represented in April–May by the model (not shown). Moreover, as seen in Figure 1a, the climatology of precipitation over India is realistic according to the climatological distribution of absorbing aerosols that also agrees with the Total Ozone Mapping Spectrometer (TOMS) satellite-derived index for absorbing aerosols [*Lau and Kim*, 2006]. We may state that overall the model used in this study meets the basic requirements for studying the impact of aerosols on Indian summer monsoon, including realistic seasonality of meteorological variables and aerosols. Figure 1a shows the climatology of precipitation over North India (averaged over the domain 70–100°E, 15–30°N) from GPCP data in the period 1986–2007 (dashed green lines) and for the 80 years of our experiment. The annual cycle of precipitation simulated by the model is in good agreement with observations in both terms of peak

intensity and seasonal evolution. ABS, which is defined by the product of the aerosol optical depth and the aerosol co-single-scattering albedo, is provided for the total optical thickness (black line). As expected, an inverse relationship is found between the model rainfall climatology and the simulated ABS due to carbonaceous and dust aerosols, with a maximum of rainfall during the peak monsoon season (July–August) that is associated with a minimum loading of aerosols. The averages of both aerosol optical depth and precipitation are computed over both land and ocean. The strong seasonality in the aerosols absorbing optical depth (black curve in Figure 1a) is due to an accumulation of aerosols in the dry season, from October to May, reaching the maximum value in April, before the start of the monsoon rainy season. The rapid removal of most of aerosols from the atmosphere corresponds to the heaviest rainfall season due to wet deposition, leading to a minimal peak of ABS in July–August. After that, the aerosol concentration increases again. To determine the contribution of different types of absorbing aerosols, the aerosol optical depth of carbonaceous particles and dust is shown in Figure 1b separately (black and green contours, respectively). Both dust and black and organic carbon are present in the same region (10–30°N, 70–100°E) for the same period (April–May) and both play an important role in the absorption optical thickness, but the ABS of dust is about 1 order of magnitude larger than that of black and organic carbon. The aerosol optical depth of BC and organic carbon in our work is smaller compared with that of *Lau et al.* [2006]. However, the magnitude of aerosol optical depth for BC in our study is in agreement with the models participating in the Aerosol Comparisons between Observations and Models (AeroCom) project, abstracted from *Kinne et al.* [2006, Table 4]. The seasonal distribution of carbonaceous aerosols shows a maximum in September–May at 15–25°N, whereas the maximum loading of dust is found in June-July-August at 20–30°N. The annual cycle of carbonaceous aerosols is due to the fact that emissions are located over the Indian subcontinent and during the wet season those aerosols are removed. On the other hand, the annual cycle of dust is instead due to transport from Thar and Middle East deserts accumulating those aerosols into the slope of the Tibetan Plateau from March to September. The circulation in March-April-May leads to transport of dust mainly from Indian and Middle East deserts, while in June-July-August there is also transport from the Thar Desert [*Lau et al.*, 2006 and *Liu et al.*, 2008]. In April–May dust and carbonaceous aerosols may be mixed in the plateau foothills both contributing to the maximum concentration of ABS in April (Figure 1a). In fact, in April–May the largest amount of absorbing aerosols measured through the simulated ABS is found over the Indo-Gangetic Plain in northern India (Figure 1c). The comparison of this pattern with the one derived from the observational TOMS aerosol index by *Lau and Kim* [2006] (see their Figure 1a) indicates a good agreement, as mentioned above. The climatological latitude-longitude distribution of the aerosol for the model simulations in April–May (Figure 1c) featuring huge amount of absorbing aerosols over the Indo-Gangetic Plain in northern India, previously identified by the ABS index, is compared with shortwave radiation in the clear sky (not shown). This comparison reveals that years with a large amount of absorbing aerosols over the Indo-Gangetic Plain in northern India correspond to years with reduced net flux at the top of the atmosphere with respect to weak aerosol loading years, indicating a larger absorption of SW radiation by the climate system in the model. The absorption of SW radiation within the atmosphere is significantly larger (on the order of 10 to 15 W/m^2), in correspondence of the region where the change in ABS is larger (not shown).

To analyze large-scale spatial variations of the Indian monsoon with the loading of absorbing aerosols, a monthly mean aerosol index defined as in *Lau and Kim* [2006] is computed averaging model ABS over the region (70–90°E, 20–30°N), where ABS climatology shows a maximum in the premonsoon season (April–May) and by considering the anomaly of the resulting time series with respect to its mean. This time series is shown in Figure 1d, and from this index we select strong (weak) years of aerosol loading corresponding to years with an amount of absorbing aerosols larger (smaller) than 1 standard deviation (reported in Figure 1d with horizontal lines). Overall we identified 12 strong and 12 weak years; these years are used to build composites of precipitation, temperature, and wind field anomalies during strong minus weak aerosol load years [*Welch*, 1938]. In our model experiment there is no correlation between the aerosols index over the selected region in South Asia and the El Niño–Southern Oscillation (ENSO) at any lag time. We further verified that strong/weak aerosol loading years do not correspond to modeled ENSO years.

Figure 2 shows the monthly composites of rainfall (shaded) and wind (vectors) in the model and in GPCP precipitation data and ERA-40 reanalysis from May to August. In the observed composites we used 1982, 1983, 1990, and 1992 as weak years and 1980, 1985, 1988, and 1991 as strong years, following the selection made by *Lau and Kim* [2006]. The spatial distribution of precipitation anomalies due to aerosols in the Asian monsoon region overlies northwestern India, the Bay of Bengal, and the northern Indian Ocean, regions of interest for the

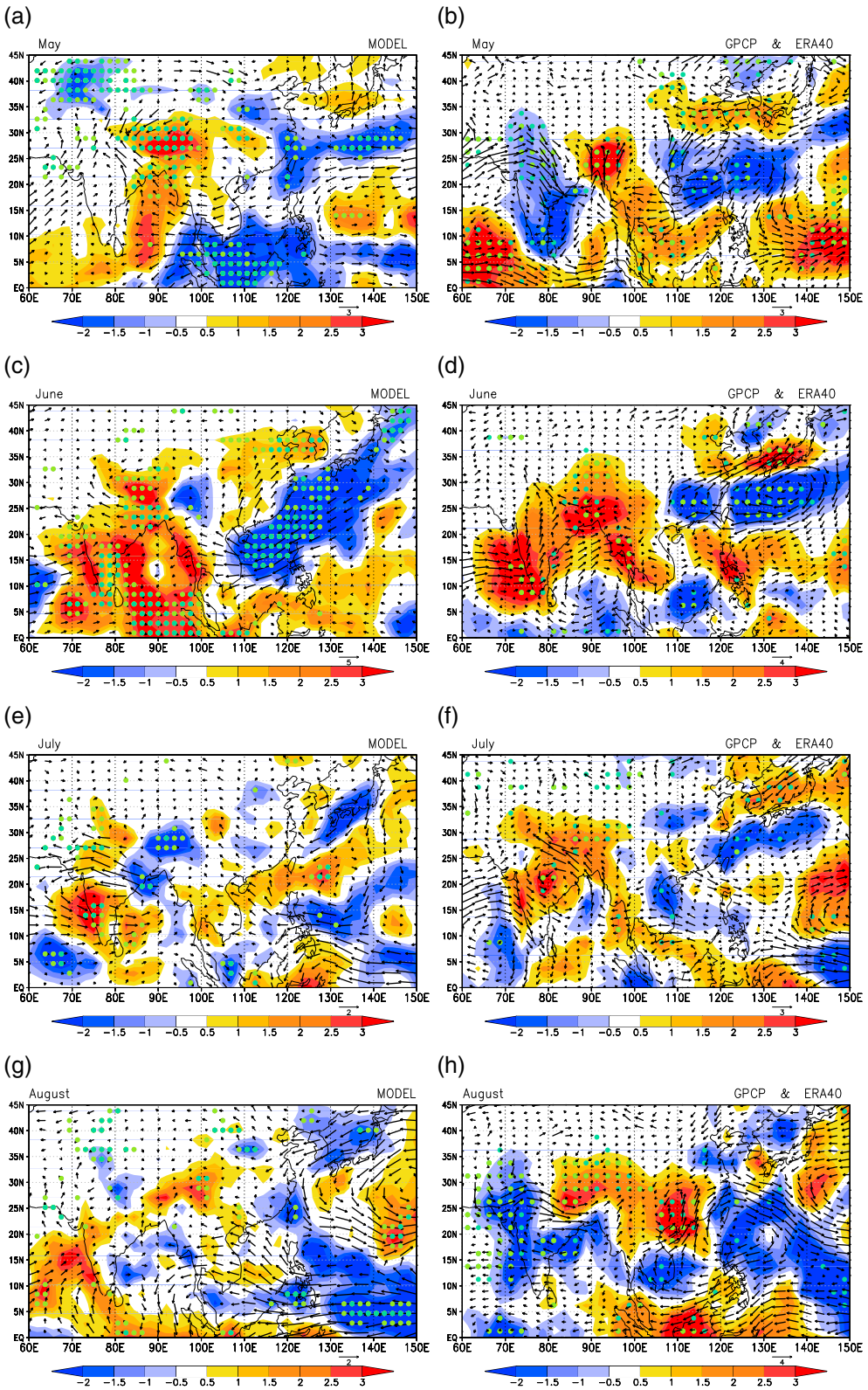

Figure 2. May-June-July-August composites of rainfall (mm d^{-1}) and 850 hPa wind pattern (m s^{-1}) for (a, c, e, and g) the model and for (b, d, f, and h) the GPCP and ERA-40. Values statistically significant at the 95% level (dark green dots) and at the 90% level (light green dots) according to a two-sample Student's *t* test are marked.

evaluation of the EHP mechanism [*Lau et al.*, 2008]. In May GPCP indicates a large decrease of precipitation over the Indian continent that is barely captured in sign by the model even though the values are not statistically significant (Figures 2a and 2b). Conversely, in the Bay of Bengal the simulated precipitation anomalies are large, positive, and significant, differently from what found in the observations (Figures 2a and 2b). In June the agreement between model and observations is wider including the significant positive anomalies in correspondence of the Tibetan Plateau, the Indian subcontinent, and the Bay of Bengal (Figures 2c and 2d), but in the model the values are slightly larger (2–2.5 mm/d) than in GPCP (1.5–2.5 mm/d). In the northern Indian Ocean the anomalies are of opposite sign when comparing model results and GPCP values (Figures 2c and 2d). In July, the precipitation anomalies over the Indian subcontinent are mostly positive and statistically significant in both model and observations at least south of 20°N (Figures 2e and 2f). The increase of precipitation in June and July is associated with an intensification of the south-westerly flow (Figures 2c–2f). In August, the anomalies become negative ($-1.5\,\mathrm{mm\,d^{-1}}$) over India and they extend up to the Arabian Sea; the model simulates negative anomalies in the eastern side of the Indian continent, but the values are weaker than observed and not statistically significant (Figures 2g and 2h). On the western side of the Indian subcontinent the anomalies are weaker than in July but still positive (Figure 2g). This month has the largest difference in terms of low-level winds between model and ERA-40 reanalysis mostly over northeast India, as for the precipitation pattern.

Increased anomalous model precipitation and stronger westerly winds at 850 hPa are indicative of enhanced Indian monsoon in early summer in the years when high aerosol loading is found in the premonsoon season, in line with the EHP hypothesis. High aerosol loading years in the model simulations are characterized by a warming of about 0.3 K in the middle and upper troposphere (Figures 3a and 3b) during premonsoon months at the foothills of Himalaya and by enhanced anticyclonic circulation (not shown) over the Tibetan Plateau. The temperature and circulation patterns are consistent with an anomalous presence of absorbing aerosols (both BC and dust) producing local atmospheric heating (Figures 4a–4h). This heating in turn results in the advection of the warmer air northward and upward over the Tibetan Plateau inducing increased temperatures, enhanced meridional temperature gradient, enhanced convection over north India, and an enhanced upper branch of the local Hadley circulation (Figures 3a and 3b). The large heating at 40–45°N in Figure 3 corresponds to the area of high concentration of dust together with black and organic carbon. In fact, the high concentration of those aerosols reaches also 40–45°N in latitude (Figure 4). However, aerosol can also induce condensation heating in regions far away from the aerosol source through dynamical feedback [*Lau et al.*, 2006].

In the model the positive feedback on increased convection and warming of the upper troposphere continues to enhance the meridional temperature gradient also in June and July (Figures 3c and 3d) leading to further strengthening of the monsoon (Figures 2c–2f), in agreement with *Lau et al.* [2006]. At the same time, the anomalies of monsoon westerly winds continue to transport more dust from the Middle East deserts toward the Indian subcontinent, although some of the aerosols are washed out because of the enhanced precipitation (Figures 4c and 4d and Figures 4g and 4h). The aerosol loading together with enhanced cloudiness associated with stronger precipitation (Figure 2) generates a surface cooling of about 1.5 K over the Indian continent, as shown in the 2 m temperature composites of both model and reanalysis (Figure 5). The cooling pattern in the model is larger; it extends also northward of 25°N, and it is statistically significant at 90%, differently from the reanalysis (Figure 5). Likely, in the reanalysis the lack of statistical significance is related with the smaller sample of years considered. Overall we cannot exclude also the influence of surface conditions, like soil moisture, known to be associated with the Indian monsoon, but the effect of soil moisture as positive or negative feedback is still matter of debate [*Meehl*, 1994]. Numerical model simulations indicate that increased moisture flux from the surface may trigger the intensity of the monsoon circulation [*Alessandri et al.*, 2007] in agreement with the monsoon land-atmosphere feedback mechanism [*Lau and Bua,* 1998]. However, even if detectable this effect seems to be less important than others [*Shukla and Mintz*, 1982; *Ferranti et al.*, 1999; *Dirmeyer*, 1999; *Douville et al.*, 2001; *Becker et al.*, 2001; *Turner and Slingo*, 2011].

To summarize, Figure 6 shows the latitude-time cross section composites of ABS over the 70–100°E sector. In years with enhanced absorption of solar radiation in the lower troposphere by carbonaceous aerosols and dust in the premonsoon season, increased precipitation over India is simulated in the model starting from April to May and peaking in June (2 mm/d). In June and July, the aerosol loading is partially reduced due to wet scavenging (Figures 4c and 4d) and the enhanced cloudiness and rainfall contribute to produce a cooling over India and a warming in the north over the Tibetan Plateau. In the peak and late monsoon season, precipitation starts to decrease in July over India (i.e., mostly north of 15°N) and then become negative in August. The cooling anomaly in June–July causes reduced precipitation in the east and north Indian

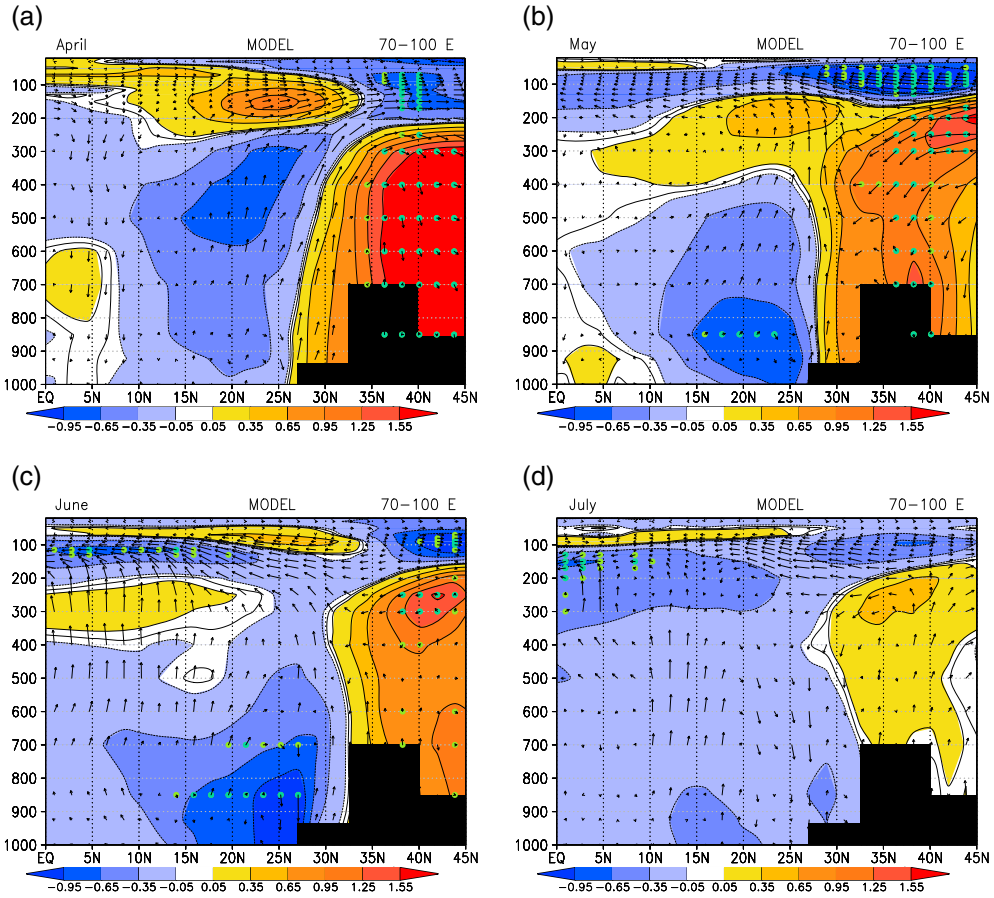

Figure 3. Latitude-height distributions of temperature (shaded) and meridional circulation (vectors) composites due to aerosols over the longitude sector of 70–100°E for (a) April, (b) May, (c) June, and (d) July. Values statistically significant at the 95% level (dark green dots) and at the 90% level (light green dots) according to a two-sample Student's *t* test are marked.

subcontinent in the following August (Figure 2g), possibly due to reduced north-south temperature gradient that impacts atmospheric stability and to reduced land evaporation [*Ramanathan et al.*, 2005; *Meehl et al.*, 2008; *Bollasina and Nigam*, 2008], consistently with a reduced monsoon circulation. The seasonality in atmospheric aerosol loading over India and Indian summer monsoon precipitation and wind effects agrees with the interpretation given by *Lau and Kim* [2010], who ascribed the increase in precipitation in the early season to the EHP mechanism and the subsequent decrease to the solar dimming effect amplified by the EHP mechanism. Our experiment with fixed external forcings reproduces in fact large-scale circulation patterns and local precipitation anomalies that are consistent with the EHP and SDM effects, suggesting that the proposed mechanisms are also acting in model simulations under constant anthropogenic aerosol emissions (the study from *Lau and Kim* [2010] was based on observed linear trends) and that the interaction of natural aerosols particularly desert dust and black carbon could be important on the seasonal-to-interannual variability of the Asian monsoon coupled atmosphere-land-ocean system. Summarizing *Lau et al.* [2006] have pointed out that such BC aerosols can combine with naturally occurring dust loading over the Tibetan Plateau to initiate the elevated heat source during the premonsoon months (March through May), thus enhancing the meridional temperature gradient and contributing to increased rainfall over India during the premonsoon and summer monsoon seasons (June–July). The complexity of aerosol monsoon interactions and the influence of aerosol impacts on monsoon rainfall have been carefully considered and discussed in detail by *Lau et al.* [2008].

4. Discussion and Conclusion

In our model setup there are two active elements that could also affect our conclusions: the presence of an active ocean and the internal variability of the coupled system, leading to oscillations such as ENSO.

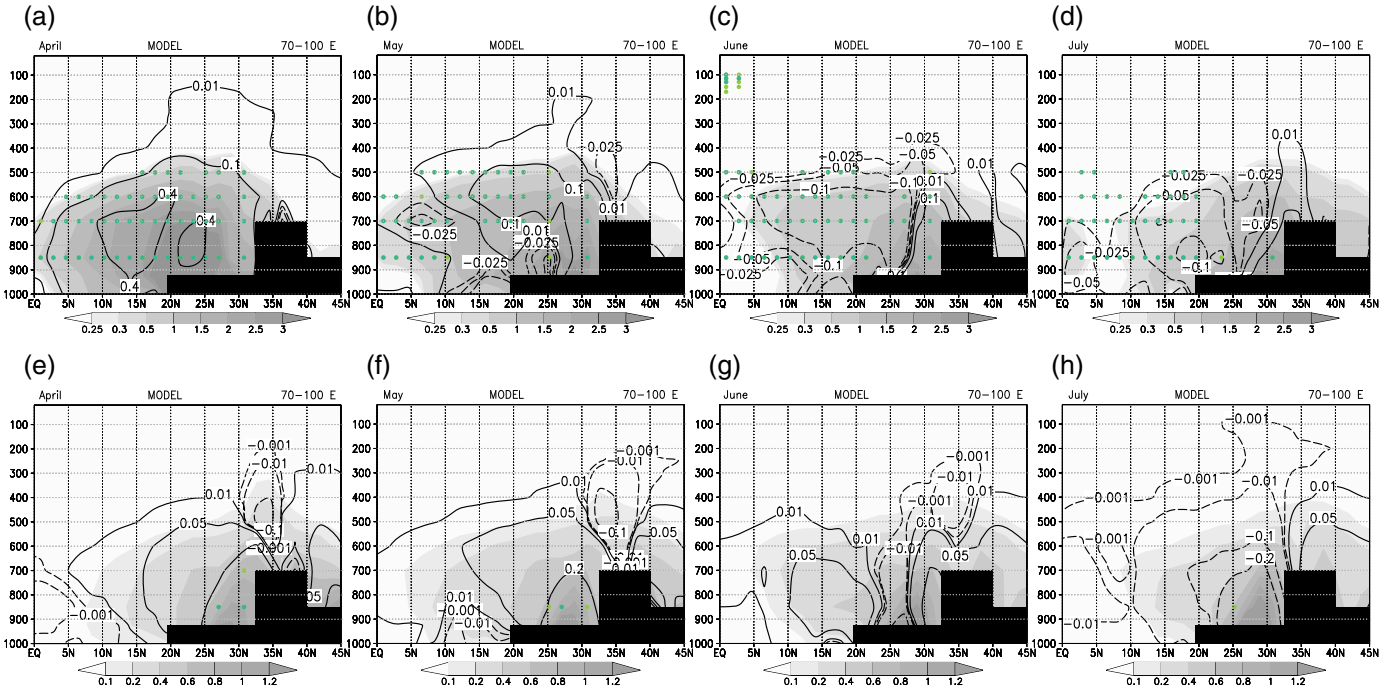

Figure 4. (a–d) Climatological latitude-height distributions of dust concentration (10^{-7} kg/kg) shaded. Composites of latitude-height distributions of positive (negative) dust concentration anomalies in solid (dashed) line. (e–h) Climatological latitude-height distributions of black and organic carbon (10^{-9} kg/kg) shaded. Composites of latitude-height distributions of black and organic carbon positive (negative) anomalies are marked with solid (dashed) lines. The data are averaged over longitudes in the sector 70°E–100°E for April, May, June, and July. Values statistically significant at the 95% level (dark green dots) and at the 90% level (light green dots) according to a two-sample Student's *t* test are marked.

Regarding ENSO we found a negative correlation between Nino-3 SST index and precipitation in summer months in agreement with previous literature using the same atmospheric model [i.e., *Cherchi and Navarra*, 2013]. In particular, in May the large significant values are mostly located over India south of 20°N and in the Indian Ocean sector surrounding the southern tip of the continent (not shown). According to this, our area of interest is mostly unaffected by this teleconnection. Further, in our model ABS and the NINO-3 indices are not significantly correlated (not shown). According to this, we can exclude a significant impact of ENSO on the relationship we found between aerosol loading years and monsoon rainfall.

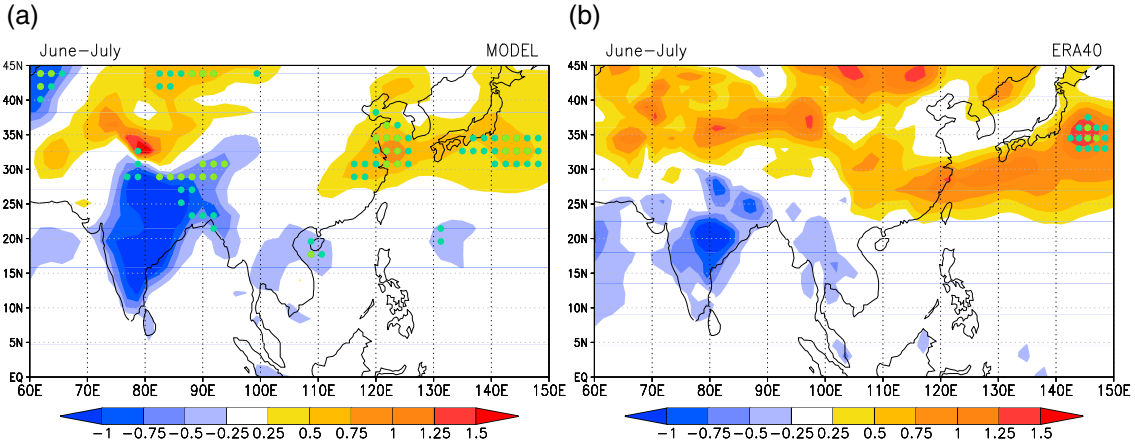

Figure 5. June–July 2 m temperature (K) composite anomalies for (a) the model and (b) ERA-40. For ERA-40 observations, the weak years (1982, 1983, 1990, and 1992) and the strong years (1980, 1985, 1988, and 1991) have been selected, following *Lau et al.* [2006]. Values statistically significant at the 95% level (dark green dots) and at the 90% level (light green dots) according to a two-sample Student's *t* test are marked.

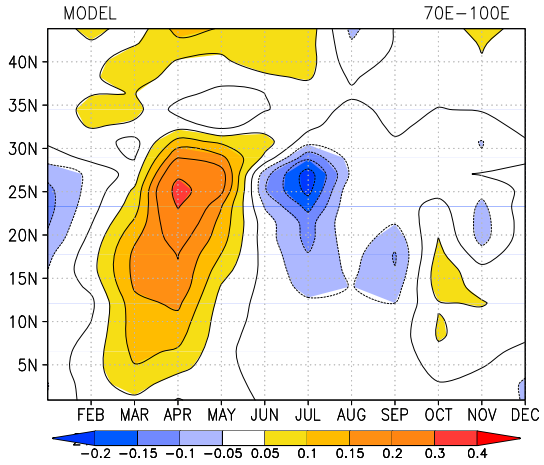

Figure 6. Time-latitude cross sections of simulated ABS annual cycle as composites of strong minus weak aerosol load years, averaged between 70°E and 100°E.

Possible effects of oceanic responses are studied by *Henriksson et al.* [2014] through mixed-layer ocean simulations and sensitivity analyses with modified fixed SSTs. In our case an interactive ocean may have some impacts, but the strength of our conclusions is guarantee by considering strong minus weak aerosols loading years.

In this work we have investigated the interaction of absorbing aerosols and the dynamics of the Indian monsoon in a coupled atmosphere-aerosol-ocean-sea ice model simulation with fixed external forcings (i.e., constant greenhouse gas and aerosol emissions from anthropogenic sources under present climate conditions). Aerosol variations in the model arise from interactive aerosol emission transport by atmospheric dynamics, dry and wet deposition. The analyses are focused on testing the validity of EHP effect in modulating seasonal to interannual variability of the Indian monsoon. The analysis is made calculating composites based on strong and weak aerosol load years over India, defined by evaluating the spatial and temporal variability of ABS. In our model setup, this classification is not completely independent from the monsoon intensity itself, as the aerosol optical depth is affected by the internal monsoon dynamics. Nevertheless, this decomposition in strong and weak aerosol loads permits to identify the changes in the monsoon characteristics associated to those years. The model includes realistic seasonality of meteorological variables and aerosols compared with observations. During the early monsoon season (April–May) enhanced absorbing aerosol loading over north India and the Himalayan foothills leads to atmospheric heating and causes, via the EHP mechanism, enhanced rainfall over South Asia and larger low-level westerly wind, in agreement with *Lau and Kim* [2006]. The simulated patterns reflect the observed composite computed using GPCP rainfall and ERA-40 wind anomalies. We find that the enhanced loading of absorbing aerosols in April–May, partially washed out in June–July, together with increased cloudiness may contribute to enhance the SDM effect leading to a subsequent cooling of the land surface in the late monsoon (July–August), both in the model and in the reanalysis (1 K and 1.5 K of cooling, respectively). In the model, the surface cooling leads to reduced local rainfall and reduced monsoon circulation over the Indian subcontinent in August associated with a reduced meridional temperature gradient and consequently reduced evaporation over land. Our results are consistent with previous analyses [*Lau and Kim*, 2006, 2010] and therefore confirm that the local distribution of aerosol and the time of the season of aerosol loading are key factors affecting local rainfall patterns over the Indian subcontinent. Given that the monsoon rainfall variability appears to be strongly dependent on premonsoon aerosol loading over northern India, our results suggest that variations of aerosol loading particularly from dust and black carbon before the monsoon onset may affect the summer rainfall and circulation variability in the Indian subcontinent at the seasonal time scale. Interestingly, even though this analysis has been performed with a set of simulations aiming at reproducing present time conditions, with fixed external forcing factors (ozone climatology, well-mixed greenhouse gases, incoming solar irradiance, and local emissions), the results are in agreement with similar composites performed with precipitation and wind data sets (GPCP and ERA-Interim) and based on a completely different index (the TOMS-derived index indirectly representing the amount of absorbing aerosols). This agreement confirms that the mechanism proposed is also operating in the model simulations. Our results therefore confirm that the local distribution of aerosols and the time of the season of aerosol loading are key factors impacting local rainfall patterns over the Indian subcontinent. These simulations have been performed with a climate model interactively coupled to an aerosol module, indicating that variations in the amount of aerosol loading before the monsoon onset may affect the intrinsic seasonal variability of the summer monsoon [see also *Vinoj et al.*, 2014; *Manoj et al.*, 2010].

Acknowledgments
The authors would like to thank the Ev-K2-CNR SHARE-PAPRIKA-Karakoram project, the Italian Ministry of Education, University and Research and the Ministry of Environment, Land and Sea through the project GEMINA, the Project of Interest Next Data of the Italian Ministry of Education, University and Research, and the FP7 INDO-MARECLIM project (295092) for financial support. Comments and suggestions from three anonymous reviewers are gratefully acknowledged. Access to the data used in this work can be provided to external users upon request to the corresponding author.

References

Adler, R. F., et al. (2003), The version-2 global precipitation climatology project (GPCP) monthly precipitation analysis (1979-present), *J. Hydrometeorol.*, *4*, 1147–1167.
Alessandri, A., S. Gualdi, J. Polcher, and A. Navarra (2007), Effects of land surface–vegetation on the boreal summer surface climate of a GCM, *J. Clim.*, *20*, 255–278, doi:10.1175/JCLI3983.1.
Becker, B. D., J. M. Slingo, L. Ferranti, and F. Molteni (2001), Seasonal predictability of the Indian summer monsoon: What role do land surface conditions play?, *Mausam*, *52*, 175–190.
Bollasina, M. A., Y. Ming, and V. Ramaswamy (2011), Anthropogenic aerosols and the weakening of the South Asian summer monsoon, *Science*, *334*(6055), 502–505, doi:10.1126/science.1204994.
Bollasina, M., and S. Nigam (2008), Indian Ocean SST, evaporation, and precipitation during the South Asian summer monsoon in IPCC-AR4 coupled simulations, *Clim. Dyn.*, doi:10.1007/s00382-008-0477-4.
Bond, T., C. Venkataraman, and O. Masera (2004), Global atmospheric impacts of residential fuels, *Energy Sustainable Dev.*, *8*(3), 20–32.
Bucci, S., C. Cagnazzo, F. Cairo, L. Di Liberto, and F. Fierli (2013), Aerosol variability and atmospheric transport in the Himalayan region from CALIOP 2007–2010 observations, *Atmos. Chem. Phys. Discuss.*, *13*, 15,271–15,299, doi:10.5194/acpd-13-15271-2013.
Cagnazzo, C., E. Manzini, M. A. Giorgetta, P. M. F. Forster, and J. J. Morcrette (2007), Impact of an improved shortwave radiation scheme in the MAECHAM5 general circulation model, *Atmos. Chem. Phys.*, *7*, 2503–2515.
Cherchi, A., and A. Navarra (2013), Influence of ENSO and of the Indian Ocean Dipole on the Indian summer monsoon variability, *Clim. Dyn.*, doi:10.1007/s00382-012-1602-y.
Collier, J. C., and G. J. Zhang (2009), Aerosol direct forcing of the summer Indian monsoon as simulated by the NCAR CAM3, *Clim. Dyn.*, *32*, 313–332, doi:10.1007/s00382-008-0464-9.
Dentener, F., et al. (2006), Emissions of primary aerosol and precursor gases in the years 2000 and 1750, prescribed data-sets for AeroCom, *Atmos. Chem. Phys. Discuss.*, *6*, 2703–2763.
Dirmeyer, P. A. (1999), Assessing GCM sensitivity to soil wetness using GSWP data, *J. Meteorol. Soc. Jpn.*, *77*, 367–385.
Douville, H., F. Chauvin, and H. Broqua (2001), Influence of soil moisture on the Asian and African monsoons. Part I: Mean monsoon and daily precipitation, *J. Clim.*, *14*(11), 2381–2403.
Dubovik, O., and M. D. King (2000), A flexible inversion algorithm for retrieval of aerosol optical properties from Sun and sky radiance measurements, *J. Geophys. Res.*, *105*, 20,673–20,696, doi:10.1029/2000JD900282.
Fan, J., L. R. Leunga, D. Rosenfeld, Q. Chen, Z. Li, J. Zhang, and H. Yan (2013), Microphysical effects determine macrophysical response for aerosol impacts on deep convective clouds, *Proc. Natl. Acad. Sci. U.S.A.*, Early Online Edition. [Available at www.pnas.org/lookup/suppl/doi:10.1073/pnas.1316830110/-/DCSupplemental.]
Ferranti, L., J. M. Slingo, T. N. Palmer, and B. J. Hoskins (1999), The effects of land-surface feedbacks on the monsoon circulation, *Q. J. R. Meteorol. Soc.*, *125*, 1527–1550.
Fogli, P. G., et al. (2009), INGV-CMCC carbon: A carbon cycle Earth system model, CMCC online RP0061. [Available at http://www.cmcc.it/publications-meetings/publications/research-papers/rp0061-ingvcmcc-carbon-icc-a-carbon-cycle-earth-system-model.]
Folini, D., and M. Wild (2011), Aerosol emissions and dimming/brightening in Europe: Sensitivity studies with ECHAM5-HAM, *J. Geophys. Res.*, *116*, D21104, doi:10.1029/2011JD016227.
Ganguly, D., P. J. Rasch, H. Wang, and J.-H. Yoon (2012), Climate response of the South Asian monsoon system to anthropogenic aerosols, *J. Geophys. Res.*, *117*, D13209, doi:10.1029/2012JD017508.
Henriksson, S. V., A. Laaksonen, V. M. Kerminen, P. Räisänen, P. H. Järvinen, A.-M. Sundström, and G. de Leeuw (2011), Spatial distributions and seasonal cycles of aerosols in India and China seen in global climate-aerosol model, *Atmos. Chem. Phys.*, *11*, 7975–7990, doi:10.5194/acp-11-7975-2011.
Henriksson, S. V., et al. (2014), Spatial distributions and seasonal cycles of aerosol climate effects in India seen in a global climate–aerosol model, *Atmos. Chem. Phys.*, *14*(18), 10,177–10,192.
Holben, B. N., et al. (2001), An emerging ground-based aerosol climatology: Aerosol optical depth from, *J. Geophys. Res.*, *106*, 12,067–12,098, doi:10.1029/2001JD900014.
Holben, B., et al. (1998), AERONET—A federated instrument network and data archive for aerosol characterization, *Remote Sens. Environ.*, *66*, 1–16.
Huang, J., P. Minnis, Y. Yi, Q. Tang, X. Wang, Y. Hu, Z. Liu, K. Ayers, C. Trepte, and D. Winker (2007), Summer dust aerosol detected from CALIPSO over the Tibetan Plateau, *Geophys. Res. Lett.*, *34*, L18805, doi:10.1029/2007GL029938.
Kinne, S., et al. (2006), An AeroCom initial assessment: Optical properties in aerosol component modules of global models, *Atmos. Chem. Phys.*, *6*, 1815–1834, doi:10.5194/acp-6-1815-2006.
Kuhlmann, J., and J. Quaas (2010), How can aerosols affect the Asian summer monsoon? Assessment during three consecutive pre-monsoon seasons from CALIPSO satellite data, *Atmos. Chem. Phys.*, *10*, 4673–4688, doi:10.5194/acp-10-4673-2010.
Lau, K. M., and W. Bua (1998), Mechanisms of monsoon-southern oscillation coupling: Insights from GCM experiments, *Clim. Dyn.*, *14*(11), 759–779.
Lau, K. M., and K. M. Kim (2011), Comment on 'Elevated heat pump' hypothesis for the aerosol-monsoon hydroclimate link: 'Grounded' in observations?" by S. Nigam and M. Bollasina, *J. Geophys. Res.*, *116*, D07203, doi:10.1029/2010JD014800.
Lau, K. M., M. K. Kim, and K. M. Kim (2006), Asian monsoon anomalies induced by aerosol direct effects, *Clim. Dyn.*, *26*, 855–864, doi:10.1007/s00382-006-0114-z.
Lau, K. M., et al. (2008), The joint aerosol-monsoon experiment: A new challenge for monsoon climate research, *Bull. Am. Meteorol. Soc.*, *89*, 369–383, doi:10.1175/BAMS-89-3-369.
Lau, K.-M., and K.-M. Kim (2006), Observational relationships between aerosol and Asian monsoon rainfall, and circulation, *Geophys. Res. Lett.*, *33*, L21810, doi:10.1029/2006GL027546.
Lau, W. K. M., and K.-M. Kim (2010), Fingerprinting the impacts of aerosols on long-term trends of the Indian summer monsoon regional rainfall, *Geophys. Res. Lett.*, *37*, L16705, doi:10.1029/2010GL043255.
Lebo, Z., and J. H. Seinfeld (2011), Theoretical basis for convective invigoration due to increased aerosol concentration, *Atmos. Chem. Phys.*, *11*, 5407–5429.
Lee, D., Y. C. Sud, L. Oreopoulos, K. M. Kim, W. K. Lau, and I. S. Kang (2014), Modeling the influences of aerosols on pre-monsoon circulation and rainfall over Southeast Asia Atmos, *Chem. Phys.*, *14*, 6853–6866, doi:10.5194/acp-14-6853-2014.
Liu, D., Z. Wang, Z. Liu, D. Winker, and C. Trepte (2008), A height resolved global view of dust aerosols from the first year CALIPSO lidar measurements, *J. Geophys. Res.*, *113*, D16214, doi:10.1029/2007JD009776.
Madec, G., and M. Imbard (1996), A global ocean mesh to overcome the north pole singularity, *Clim. Dyn.*, *12*, 381–388.

Madec, G., P. Delecluse, I. Imbard, and C. Levy (1999), OPA 8.1 ocean general circulation model reference manual, Note du Pôle de modélisation No. 11, Inst. Pierre-Simon Laplace (IPSL), France, 91 pp.
Mann, G. W., et al. (2014), Intercomparison and evaluation of global aerosol microphysical properties among AeroCom models of a range of complexity, *Atmos. Chem. Phys.*, *14*, 4679–4713, doi:10.5194/acp-14-4679-2014.
Manoj, M. G., P. C. S. Devara, P. D. Safai, and B. N. Goswami (2010), Absorbing aerosols facilitate transition of Indian monsoon breaks to active spells, *Clim. Dyn.*, *37*, 2181–2198.
Meehl, G. A. (1994), Coupled land-ocean-atmosphere processes and south Asian monsoon variability, *Science*, *266*, 263–267.
Meehl, G. A., J. M. Arblaster, and W. D. Collins (2008), Effects of black carbon aerosols on the Indian monsoon, *J. Clim.*, *21*, 2869–2882.
Menon, S., J. E. Hansen, L. Nazarenko, and Y. Luo (2002), Climate effects of black carbon aerosols in China and India, *Science*, *297*, 2250–2253, doi:10.1126/science.1075159.
Nigam, S., and M. Bollasina (2010), "Elevated heat pump" hypothesis for the aerosol-monsoon hydroclimate link: "Grounded" in observations?, *J. Geophys. Res.*, *115*, D16201, doi:10.1029/2009JD013800.
Ramanathan, V., et al. (2001), Indian Ocean Experiment: An integrated assessment of the climate forcing and effects of the great Indo-Asian haze, *J. Geophys. Res.*, *106*(D22), 28,371–28,398, doi:10.1029/2001JD900133.
Ramanathan, V., et al. (2005), Atmospheric brown clouds: Impact on South Asian climate and hydrologic cycle, *Proc. Natl. Acad. Sci. U.S.A.*, *102*, 5326–5333.
Randles, C. A., and V. Ramaswamy (2008), Absorbing aerosols over Asia: A Geophysical Fluid Dynamics Laboratory general circulation model sensitivity study of model response to aerosol optical depth and aerosol absorption, *J. Geophys. Res.*, *113*, D21203, doi:10.1029/2008JD010140.
Roeckner, E., R. Brokopf, M. Esch, M. Giorgetta, S. Hagemann, L. Kornblueh, E. Manzini, U. Schlese, and U. Schulzweida (2006), Sensitivity of simulated climate to horizontal and vertical resolution in the ECHAM5 atmosphere model, *J. Clim.*, *19*, 3771–3791.
Schulz, M., G. de Leeuw, and Y. Balkanski (2004), Sea-salt aerosol source functions and emissions, in *Emission of Atmospheric Trace Compounds*, edited by C. Granier, P. Artaxo, and C. E. Reeves, pp. 333–359, Kluwer Acad., Dordrecht, Netherlands.
Scoccimarro, E., S. Gualdi, A. Bellucci, A. Sanna, P. G. Fogli, E. Manzini, M. Vichi, P. Oddo, and A. Navarra (2011), Effects of tropical cyclones on ocean heat transport in a high resolution coupled general circulation model, *J. Clim.*, *24*, 4368–4384.
Shukla, J., and Y. Mintz (1982), Influence of land-surface evapotranspiration and the Earth's climate, *Science*, *219*, 1498–1501.
Stier, P., et al. (2005), The aerosol-climate model ECHAM5-HAM, *Atmos. Chem. Phys.*, *5*, 1125–1156.
Stier, P., J. H. Seinfeld, S. Kinne, and O. Boucher (2007), Aerosol absorption and radiative forcing, *Atmos. Chem. Phys.*, *7*, 5237–5261, doi:10.5194/acp-7-5237-2007.
Tao, W. K., J. P. Chen, Z. Li, C. Wang, and C. Zhang (2012), Impact of aerosols on convective clouds and precipitation, *Rev. Geophys.*, *50*, RG2001, doi:10.1029/2011RG000369.
Tegen, I., S. P. Harrison, K. Kohfeld, I. C. Prentice, M. Coe, and M. Heimann (2002), Impact of vegetation and preferential source areas on global dust aerosols: Results from a model study, *J. Geophys. Res.*, *107*(D21), 4576, doi:10.1029/2001JD000963.
Tegen, I., M. Werner, S. P. Harrison, and K. E. Kohfeld (2004), Relative importance of climate and land use in determining present and future global soil dust emission, *Geophys. Res. Lett.*, *31*, L05105, doi:10.1029/2003GL019216.
Timmermann, R., H. Goosse, G. Madec, T. Fichefet, C. Ethé, and V. Dulière (2005), On the representation of high latitude processes in the ORCA-LIM global coupled sea ice ocean model, *Ocean Model.*, *8*, 175–201.
Toon, O. B., and T. P. Ackerman (1981), Algorithms for the calculation of scattering by stratified spheres, *Appl. Opt.*, *20*(20), 3657–3660.
Turner, A. G., and H. Annamalai (2012), Climate change and the South Asian summer monsoon, *Nat. Clim. Change*, *2*, 1–9.
Turner, A. G., and J. M. Slingo (2011), Using idealized snow forcing to test teleconnections with the Indian summer monsoon in the Hadley Centre GCM, *Clim. Dyn.*, *36*(9–10), 1717–1735.
Uppala, S. M., et al. (2005), The ERA-40 re-analysis, *Q. J. R. Meteorol. Soc.*, *131*, 2961–3012, doi:10.1256/qj.04.176.
Valcke, S. (2006), *OASIS3 User Guide (prism_2-5)*, *PRISM Report No 2*, 6th ed., 64 pp., CERFACS, Tolouse, France.
Van Der Werf, G. R., et al. (2003), Carbon emissions from fires in tropical and subtropical ecosystems, *Global Change Biol.*, *9*(4), 547–562.
Vinoj, V., J. P. Rasch, H. Wang, J.-H. Yoon, P.-L. Ma, K. Landu, and B. Singh (2014), Short-term modulation of Indian summer monsoon rainfall by West Asian dust, *Nat. Geosci.*, doi:10.1038/NGEO2107.
Wang, C., D. Kim, A. M. L. Ekman, M. C. Barth, and P. J. Rasch (2009), Impact of anthropogenic aerosols on Indian summer monsoon, *Geophys. Res. Lett.*, *36*, L21704, doi:10.1029/2009GL040114.
Welch, B. L. (1938), The significance of the difference between two means when the population variance are unequal, *Biometrika*, *29*(3/4), 350–362.